Finite Element Approach for the Analysis of the Fuel Cell Internal Stress Distribution

E. Firat*[,1,2], P. Beckhaus[1], A. Heinzel[1,2]
[1]Center for Fuel Cell Technology (ZBT) GmbH, Duisburg
[2]University of Duisburg Essen
*Corresponding author: Zentrum für BrennstoffzellenTechnik (ZBT) GmbH Carl-Benz-Straße 201, D-47057 Duisburg, Germany, e.firat@zbt-duisburg.de

Abstract: The mechanical durability of fuel cell stack components is essential for the safe operation and extension of the product lifespan. Getting an even internal stress distribution for each cell is one design criterion which directly affects fuel cell performance. Clamping the fuel cell stack with tie-rods is a common method for compression of fuel cells. To analyze the mechanical effect of the clamping on the single cell components a 3D model has been set-up and solved using COMSOL Multiphysics®. Implementation of the thermal expansion into the structural module for each component allows to evaluate the stress distribution in the fuel cell during variation of operating conditions. The large-scale 3D FEM (Finite Element Method) analysis helps with the understanding of the stack design and dimensioning of the components from a mechanical point of view.

Keywords: Polymer-electrolyte-membrane fuel cell (PEMFC), fuel cell mechanics, stack design

1. Introduction

A single fuel cell consists of the components shown in Figure 1. The fuel cells components have to be held mechanically together to prevent leakage and ensure good electrical conductivity, both of which play an important role in fuel cell performance [1-3]. Gas leakages in fuel cells cause not only performance losses but also lead to potentially dangerous situations [4]. A fuel cell stack, which is an assembly of a number of single fuel cells, has to ensure above-mentioned properties for each cell. Compressing the fuel cells with the help of two endplates and clamping them with tie rods is a conventional method used in fuel cell stack design. The requirement for fas tightness and low contact resistance result in high compression pressure values for stack design. However over-compressing of fuel cell components such as the gas diffusion layer (GDL) disturbes their porous structures thus reduces the performance of a fuel cell [5]. It can also cause cracking of the bipolar plates (BPP) due to the brittleness of the graphite based plates [6]. The realization of a uniform internal stress distribution for each cell component is therefore essential [7]. As a result of prior work, it is well known that the stack design parameters affect the performance of a PEMFC and its product lifespan directly.

In this study, COMSOL Multiphysics® is used to analyze the fuel cell stack design from a mechanical point of view. A 3D model representing a fuel cell stack with 5 cells is precisely established and carefully meshed with regard to the stress configuration. Additionally, the computation of thermal expansion for each component is also taken into account by integrating cell operating temperature profiles into the structural module. The material properties of the components are assumed to be independent of temperature. Understanding the fuel cell stack design on a large scale from a mechanical point of view contributes to the optimization of the stack design and dimensioning of the components.

2. Use of COMSOL Multiphysics®

In contrast to other computing interfaces COMSOL Multiphysics® has multiphysics capabilities. The ability to add dependent variables facilitates the proper analysis of the engineering systems.

2.1. Model Set-up

A fuel cell stack consists of the following components shown in Figure 1. Excluding the catalyst layers and very small fillets for flow fields, the FEM model is derived in accordance with the original models. The very thin catalyst layers and very small fillets for flow fields are neglected regarding their trivial contributions to the mechanical properties.

By taking advantage of symmetry and antisymmetry conditions, only one eighth of the 3D model is used, thus resulting in the reduction of computation time. The complexity of the 3D model analysis is achieved by using the assembly structure and the implementation of identity pairs, which enables the components to be meshed separately [8]. Disc springs are removed from the FEM model under the

assumption of direct transformation of axial loads on washers.
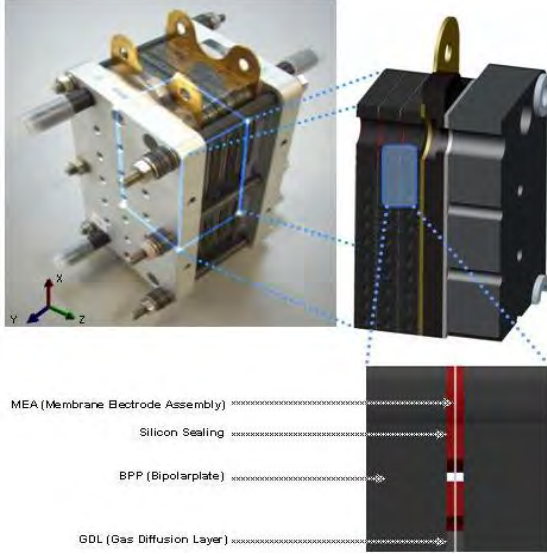
Figure 1 Stack with 5 cells and FEM model

2.2. Subdomain Equations

To analyze the effect of thermal expansion, structural and thermal-structural computations are performed separately. The governing equation for structural mechanics is shown in Eq.(1). It is derived from the equation of motion with regard to the equilibrium condition (for further information [9-10]).

$$\nabla \cdot (D\nabla \underline{\mathbf{u}}) = 0 \qquad \text{Eq.(1)}$$

$\underline{\mathbf{u}}$, D (defined in Eq.(2)) denote the displacement vector and stiffness matrix for isotropic materials respectively [11].

$$D = \frac{E}{(1+v)(1-2v)} \begin{bmatrix} 1-v & v & v & 0 & 0 & 0 \\ v & 1-v & v & 0 & 0 & 0 \\ 0 & 0 & 0 & \frac{1-2v}{2} & 0 & 0 \\ 0 & 0 & 0 & 0 & \frac{1-2v}{2} & 0 \\ 0 & 0 & 0 & 0 & 0 & \frac{1-2v}{2} \end{bmatrix} \qquad \text{Eq.(2)}$$

E represents the young modulus and v is Poisson's ratio. Considering the anisotropy of the GDL in the through plane direction as depicted in [12], the orthotropic material

properties are used for the regarding components (for further information see [11]). The Young Modulus defined as a function of strain in the y axis (ε_y) can be found in Subsection 2.4 (Material Properties).

The governing equations for the heat transfer are shown in Eq.(3) and Eq.(4) without and with convection respectively.

$$\nabla \cdot (-k\nabla \mathbf{T}) = Q \qquad \text{Eq.(3)}$$

$$\nabla \cdot (-k\nabla \mathbf{T}) = Q - \rho C_p \underline{u}.\nabla \mathbf{T} \qquad \text{Eq.(4)}$$

The thermal simulation represents the stationary conditions regarding the thermal expansion purpose. The calculated $\mathbf{T}$ in Eq.(3) is used in the structural mechanics module with the reference ambient temperature of 23˚C. The strain consists of thermal ε_{th}, elastic ε_{el} and initial strain ε_0 contributions as indicated in the Eq.(5) [11].

$$\varepsilon = \varepsilon_{el} + \varepsilon_{th} + \varepsilon_0 \qquad \text{Eq.(5)}$$

2.3. Boundary Settings

The axial force acting on washers is calculated for each bolt as 1260 [N] according to [13]. The acting axial forces by grub screws are also calculated as 640 [N] for each one. The constraints are applied as XY, XZ and YZ symmetry conditions on the respective surfaces. This also leads to the point symmetry of the fuel cell stack in the middle.

For the thermal boundary settings the fuel cell stack operation temperature is used. The generated heat power (Q_{gen}) is calculated as 19.63 [W] according to the Eq.(6) [2, 14] on the basis of the theoretical potential (1.482 [V]), cell voltage (V_{cell}) and the stack current (I). Q_{gen} is then implemented as the heat source in the model. For the definition of the convection condition at the outer surfaces, the COMSOL Multiphysics® library is used [20].

$$Q_{gen} = (1.482[V] - V_{cell})I \cdot n_{cell} \qquad \text{Eq.(6)}$$

2.4. Material Properties

The components and material properties of a fuel cell stack are listed in Table 1.

Table 1: Component and material list

Material Properties	Unit	Value	Source
Alu-5083			
Young Modulus	[GPa]	70.3	[15]
Poisson's ratio		0.33	[15]
Specific Heat(Cp)	[J/kg.K]	900	[15]
Thermal Conductivity	[W/m.K]	117	[15]
Density	[kg/m³]	2660	[15]
Thermal Exp.	10^{-6} [1/°C]	23.8	[15]
BPP-Graphite-Compound			
Young Modulus	[GPa]	15.56	[16,17]
Poisson`s ratio		0.25	[18]
Specific Heat(Cp)	[J/kg.K]	685	[21]
Thermal Conductivity	[W/m.K]	25,15,25	[16]
Density	[kg/m3]	1770	[16]
Thermal Exp.	10^{-6} [1/°C]	12.2	[16]
Copper			
Young Modulus	[GPa]	110	[20]
Poisson`s ratio		0.35	[20]
Specific Heat(Cp)	[J/kg.K]	385	[20]
Thermal Conductivity	[W/m.K]	400	[20]
Density	[kg/m3]	8700	[20]
Thermal Exp.	10^{-6} [1/°C]	17.00	[20]
Dry GDL			
Young Modulus	[GPa]	10, $f(\varepsilon_y)$, 10	[12, 18]
Poisson`s ratio		0.25, 0, 0.25	[12, 18]
Specific Heat(Cp)	[J/kg.K]	685	[21]
Thermal Conductivity	[W/m.K]	21,1.7,21	[22]
Density	[kg/m3]	2045	[21]
Thermal Exp.	10^{-6} [1/°C]	-0.8	[22]
Nafion-N-112			
Young Modulus	[GPa]	0.249	[23]
Poisson`s ratio		0.25	[18]
Specific Heat(Cp)	[J/kg.K]	4188	[21]
Thermal Conductivity	[W/m.K]	0.18	[21]
Density	[kg/m3]	1961	[23]
Thermal Exp.	10^{-6} [1/°C]	123	[18]
Polycarbonate			
Young Modulus	[GPa]	2.38	[19]
Poisson`s ratio		0.36	[19]
Specific Heat(Cp)	[J/kg.K]	840	[19]
Thermal Conductivy	[W/m.K]	0.2	[19]
Density	[kg/m3]	1200	[19]
Thermal Exp.	10^{-6} [1/°C]	122	[19]
Silicon			
Young Modulus	[GPa]	131	[20]
Poisson`s ratio		0.27	[20]
Specific Heat(Cp)	[J/kg.K]	703	[20]
Thermal Conductivity	[W/m.K]	163	[20]
Density	[kg/m3]	2330	[20]
Thermal Exp.	10^{-6} [1/°C]	4.15	[20]
Steel 1.4307-ASI 304			
Young Modulus	[GPa]	193	[19]
Poisson`s ratio		0.3	[19]
Specific Heat(Cp)	[J/kg.K]	500	[19]
Thermal Conductivity	[W/m.K]	16.2	[19]
Density	[kg/m3]	8000	[19]
Thermal Exp.	10^{-6} [1/°C]	17.2	[19]

The anisotropy of the GDL is also considered regarding its composite material structure. GDL has an important task on the fuel cell performance and a direct influence on the fuel cell internal stress distribution as explained before. [12] shows that GDL has anisotropic material properties in the through plane direction. Compression stiffness of the GDL increases as a result of the molecular structure. The thickness of a dry GDL (Toray Carbon Paper) has been measured with an INSTRON testing instrument (Figure 2) [16]. Using MATLAB® script, the corresponding Young Modulus is derived as a function (Eq.(7)) of the through plane strain.
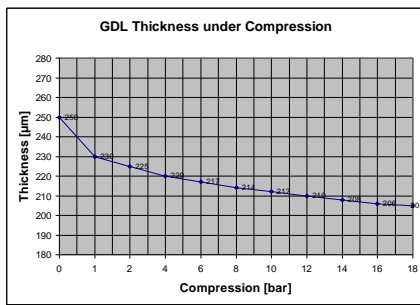
Figure 2 GDL Thickness under compression

$$f(\varepsilon_y) = (0.49 e^9 \varepsilon_y^2) - (0.041 e^9 \varepsilon_y) \quad \text{Eq.(7)}$$

The function is implemented as a subdomain equation for GDL and assigned to GDL orthotropic material properties.

2.5. Meshing and Solver Settings
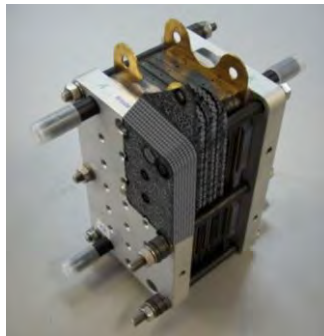
Figure 3 Meshing elements

Mapped, swept and free meshing options are utilized depending on geometry, stress configuration and state of concern. Meshing of the one-eighth model can be seen in Figure 3. The meshing properties for both structural and thermal-structure computations can be seen in Table 2.

Table 2 Meshing properties

	Number of Elements	Degree of Freedom	Element Quality
Structure	238108	399879	0.0153
Thermal-Structure	238108	952729	0.0153

The meshing properties are kept the same for both structural and thermal-structural computations.

The element type for each geometry is selected as linear or quadratic considering the simulation conditions. This can be seen from the degree of freedom number listed in Table 2.

With regard to the complexity of the 3D model and the amount of the degree of freedom, a direct solver (SPOOLES) is chosen. For the computations including both thermal and structural analysis, a segregated solver is selected. In segregated solver, the direct solver (SPOOLES) is assigned to both modules for the computation of the variables.

3. Results

The simulated temperature profile can be depicted from Figure 4. The temperature profile decreases drastically through the isolation plate as expected. The temperature profile can also be revised and be improved by optimizing the thermal constraints.
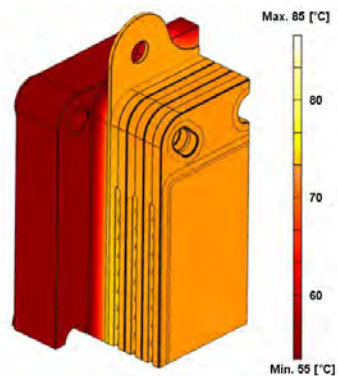
Figure 4 Temperature profile [C] of Stack

4

In Figure 5 the total displacement can be seen for both structural (a) and thermal-structural (b) analysis in scaled sizes. Owing to the simulation results, the stack design can be analyzed with and without fuel cell operating conditions.
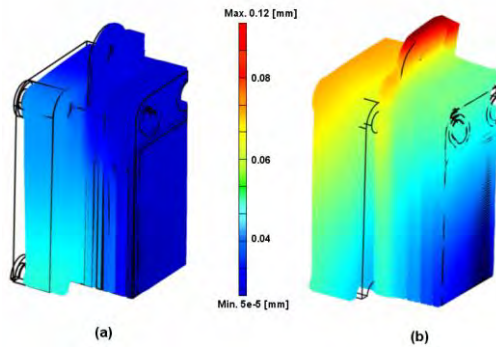
Figure 5 Total displacement [mm] for both structural (a) and thermal-structural (b) analysis

The accumulating thermal expansion of the stack components results in a change in the displacement profile of the fuel cell stack as seen in the Figure 5 (a) - (b) The thermal elongation against the compression direction results as a change of the total displacement profile. It can be seen in Figure 5 that the use of grub screws supports the stack against elongation caused by thermal expansion from design point of view.

In Figure 6, global normal stress on the membrane in y-axis can be seen for both structural and thermal-structural analysis. The other components are suppressed. Because of the sealing gaskets, the global normal stress intensifies on the outer surface.
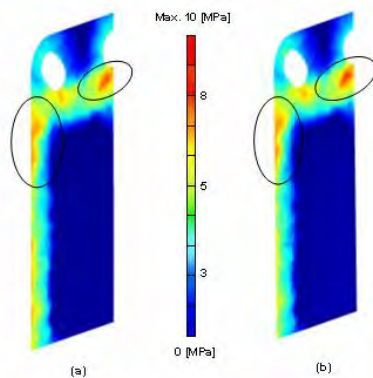
Figure 6 Global normal stress [MPa] on membrane for structural (a) and thermal-structural analysis (b)

The average stress on the membrane is calculated as 2.40 [MPa] (structural) and 2.42 [MPa] (thermal-structural) by using the boundary integration for corresponding surfaces.

In Figure 6, areas circled in black are the critical regions differing slightly from structural to thermal-structural analysis. The critical gasket zones can lead to tightness problems during the operations.

In Figure 7 Von Mises stress on the membrane can be seen for both structural and thermal-structural analysis. The stress distribution is slightly compensated by thermal expansion.
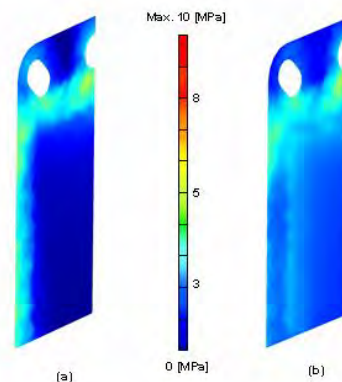
Figure 7 Von Mises Stress [MPa] on membrane for structural (a) and thermal-structural analysis (b)

In Figure 8, the through plane (y-axis) displacement on the GDL can be figured out along the body axis (z-axis in the middle) for structural analysis.
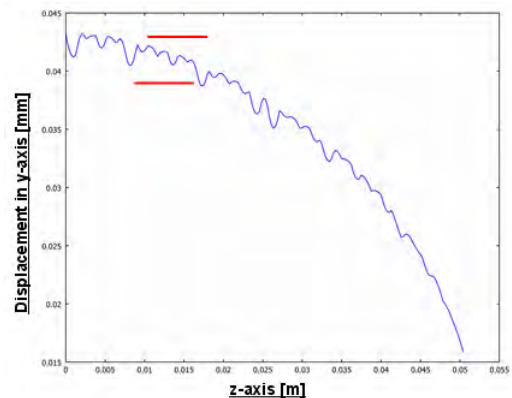
Figure 8 Through plane displacement in the middle (in x-axis) of GDL along the body axis (in z-axis) for structural analysis

The peaks in Figure 8 correspond to the GDL squeezed into the flow field channels. The squeezing of the GDL into flow fields differs from channel to channel. The large-scale analysis contributes to understanding of squeezing of GDL for each flow field.
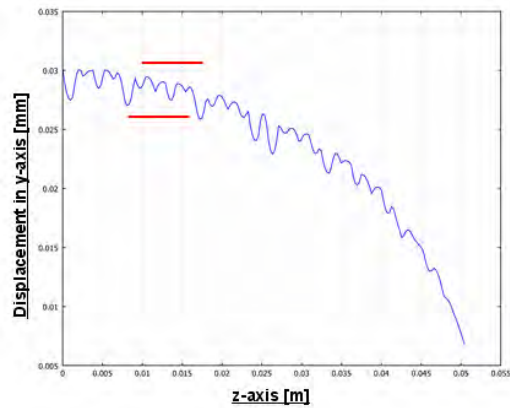
Figure 9 Through plane displacement in the middle (in x-axis) of GDL along the body axis (in z-axis) for structural analysis

In Figure 9 the through plane (y-axis) displacement on the GDL can be figured out along the body axis (z-axis in the middle) for thermal-structural analysis. The thermal expansion contributes to additional displacement through the body which results as homogenization of the total displacement profile. The squeezing changes along the z axis because of the increase of total displacement through the top of the fuel cell stack. Different from the structural analysis the thermal expansion contributes to the compensation of the displacement on the GDL. But the squeezing factor and the tendency remain the same.
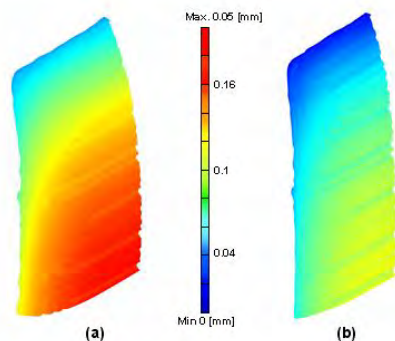
Figure 10 Through plane displacement [mm] on GDL for both Structural (a) and Thermal-Structural (b) Analysis

In Figure 10 the scaled through plane displacement of a GDL is visualized for structural and thermal-structural analysis. The squeezing of the GDL into the flow field channels and flow field structure can be simply captured. The thermal expansion affects the through plane displacement of the GDL directly. The optimization of the thermal computations provides better understanding of squeezing of the GDL.

4. Conclusion

In this study, the state of design for the 50 cm^2 fuel cell stack of The Center for Fuel Cell Technology (ZBT) in Duisburg is analyzed from a mechanical point of view. The dynamic temperature profile in fuel cells occurring in operating conditions plays an important role in stack design. The temperature profiles for PEM fuel cells are relatively small. But with regard to the size and sensitivity of components it must also be taken into consideration in the field of stack design. The high thermal expansion coefficient values of some components such as isolation plates contribute to noticeable strain changes. Neglecting other properties affecting the mechanical properties e.g. humidity, the fuel cell stack design is analyzed with and without thermal expansion. The boundary conditions can also be revised and improved.

The large-scale analysis of the fuel cell stack facilitates to evaluate the stack design as a whole. The effect of design parameters on single components can also be figured out. Understanding the mechanical effect of the components such as endplates on the design objectives contributes to the optimization procedure. It is experienced that the material properties and the anisotropy of the single components play an important role in performing the computations even on large-scale.

The material properties can also be improved by considering other properties affecting the mechanical properties.

The study of the thermal management can also be improved defining an optimized heat source term.

5. References

1. Wang, X., Song, Y., Zhang, B., Experimental Study on Clamping Pressure Distribution in PEM Fuel Cells, *J. Power Sources*, **179**, 305-309 (2008)

2. Barbir, Frano, PEM Fuel Cells-Theory and Practic, Elsevier Academic Press, page: 178-197 (2005)

3. Lu, Z., Kim, C., Karlsson, A. M., Cross III, J. C., Santare, M.H., Effect of Gas Diffusion Layer Modulus and Land-Groove Geometry on Membrane Stresses in Proton Exchange Membrane Fuel Cells, *J. Power Sources*, **196**, 4646-4654 (2011)

4. Jiabin, G., Higier, A., Liu, H., Effect of Gas Diffusion Layer Compression on PEM Fuel Cell Performance, *J. Power Sources*, **159**, 922-927 (2006)

5. Xing, X. Q., Lum, K. W., Poh, H.J., Wu, Y. L., Optimization of assembly Clamping Pressure on Performance of Proton-Exchange membrane Fuel Cells, *J. Power Sources*, **195**, 62-68 (2010)

6. Zhou, Y., Lin, G., Shih, A.J., Hu, S. J., Multiphysics Modeling of Assembly Pressure Effects on Proton Exchange Membrane Fuel Cell Performance, *J. Fuel Cell Sci. Technol.*, **6**, 041005-1(2009)

7. Montanini, R., Squadrito, G., Giacoppo, G., *XIX IMEKO World Congress Fundamental and Applied Metrology, September* **6-11**, (2009)

8. Comsol User Guide, page: 92, (2008)

9. Pepper, W., Heinrich, J.C., The Finite Element Method, Basic Concepts and Applications, (1992)

10. Von Mark S. Gockenbach, Partial differential equations: analytical and numerical methods, (2002)

11. Comsol Structural Mechanics Module User`s Guide, pg.179 (2008)

12. Kleemann, J., Finsterwalder, F., Tillmetz, W., Characterization of Mechanical Behavior and Coupled Electrical Properties of Polymer Electrolyte Membrane Fuel Cell Gas Diffusion Layers, *J. Power Sources*, **190**, 92-102 (2009)

13. VDI-Richtlinie 2230; Systematische Berechnung hochbeanspruchter Schraubenverbindungen (Abschnitt 13.1.9)

14. Kreuz, C., PEM-Brennstoffzellen mit Spritzgegossenen Bipolarplatten aus hochgefülltem Graphit-Compound, Universität Duisburg-Essen, Dissertation, (2008)COMSOL Heat Transfer Module User's Guide, page: 65, (2008)

15. http://www.matweb.com

16. ZBT GmbH (Zentrum für Brennstoffzellen-technik in Duisburg)-Center for Fuel Cell Technology in Duisburg

17. DIN EN ISO 178, Kunststoffe-Bestimmung der Biegeeigenschaften (ISO 178:2010); Deutsche Fassung EN ISO 178:2010

18. Otmani, N., Morin, A., Di Iorio, S., Rouillon, L., Delette, G., Blachot, J.F., Gebel, G., Besse, S., Stresses in Nafion® Membranes During Fuel Cell Operation, *Fundamentals and Developments of Fuel Cells Con.*, (2008)

19. Callister, J.D. W., Materials Science and Engineering an Introduction, John Wiley & Sons Inc., Page: 789-816, (2000)

20. Comsol Material Library COMSOL Multiphysics® (3.5a)

21. Shah, A. A., Ralph, T. R., Walsh, F. C., Modeling and Simulation of the Degradation of Perfluorinated Ion-Exchange Membranes in PEM Fuel Cells, *J.Electrochem. Soc.*, **156**, (4) B465-B484 (2009)

22. Toray Industries, Inc.

23. E. I. du Pont de Nemours and Company